Accelerated Publications

Electrochromic Detection of a Coherent Component in the Formation of the Charge Pair $P^+H_L^-$ in Bacterial Reaction Centers†

Marten H. Vos,*,‡ Christian Rischel,§ Michael R. Jones,|| and Jean-Louis Martin‡

INSERM U451, Laboratoire d'Optique Appliquée, Ecole Polytechnique-ENSTA, 91761 Palaiseau Cedex, France, Department for Mathematics and Physics, Royal Veterinary and Agricultural University, Thorvaldsensvej 40, DK-1871 Frederiksberg C, Denmark, Niels Bohr Institute, Blegdamsvej 17, DK-2100 Copenhagen, Denmark, and Department of Biochemistry, School of Medical Sciences, University of Bristol, University Walk, Bristol BS8 1TD, United Kingdom

Received April 4, 2000; Revised Manuscript Received May 23, 2000

ABSTRACT: We demonstrate coupling of an intraprotein electron transfer reaction to coherent vibrational motions. The kinetics of charge separation toward the radical pair state $P^+H_L^-$ were studied in reaction centers of *Rhodobacter sphaeroides* at 15 K. The electrochromic shift of the bacteriochlorophyll monomers is the most prominent spectral feature associated with this charge displacement. The newly reported absolute absorption spectrum of the $P^+H_L^-$ state is discussed in terms of this shift. In wild-type reaction centers, the rise kinetics of the electrochromic shift display a small but significant 30 cm^{-1} periodic modulation (period of ∼1 ps). This modulation is also present in FL181Y mutant reaction centers, where overall charge separation is somewhat more rapid than in the wild-type reaction center. In contrast, in YM210L mutant reaction centers, where the charge separation is much slower, the modulation is absent. The conclusion that the motion along the reaction coordinate has a 30 cm^{-1} coherent component is discussed in light of possible mechanisms of electron transfer.

In recent years, femtosecond coherence spectroscopy has been developed as a new tool for detecting low-frequency nuclear motion in protein systems that can be activated by light (*1*). In such systems, impulsive photoexcitation populates an off-equilibrium configuration on the potential energy surfaces of a ground state, excited state, and, possibly, a subsequent product state. The coherent vibrations thus set in motion give rise to oscillatory modulation of the absorption or emission spectra of the respective states. As examples of the observation of such motions, we mention ground state motions in bacteriorhodopsin (*2*), excited state motions in bacterial reaction centers (*3*), and product state motions in rhodopsin (*4*) and myoglobin (*5*).

Apart from providing a tool for vibrational spectroscopy, coherent signals can be used to determine motions that drive intraprotein reactions. In this way, we have recently demonstrated "stepwise" reaction dynamics during ligand transfer in cytochrome *c* oxidase (*6*). In this report, we investigate the involvement of vibrations in an ultrafast electron transfer (ET)[1] reaction. The possibility that nuclear motions drive coherent displacement of charges has been examined in theoretical work (*7*−*16*).

Unambiguous detection of charge movements requires an electric field-sensitive probe that is spectrally separated from the transitions that probe the potential energy surfaces where the nuclear motions occur. The photosynthetic reaction center (RC) (*17*) from *Rhodobacter sphaeroides* offers an opportunity to achieve this by monitoring the electrochromic shifts of the bacteriochlorophyll (BChl) monomer cofactors (denoted B). These are located close to the cofactors that participate in the reactant excited state P* and product radical pair state $P^+H_L^-$ (P, bacteriochlorophyll dimer primary donor; H_L, bacteriopheophytin acceptor) of primary charge separation (Figure 1A). This charge separation takes place within a few picoseconds (*18*−*20*). In femtosecond experiments, coherences have been observed in the region of the neutral ground state absorption of the B cofactors, near 800 nm (*3*, *21*−*25*), and in a region near 1020 nm that is ascribed to a BChl anion intermediate (*26*, *27*). In both of these regions, relatively strong contributions arising from vibrational modes associated with the P* state are present. We have recently shown (*21*) that a relatively "clean" spectral area is provided by the positive, blue lobe of the band-shift

† M.H.V. is supported by CNRS. M.R.J. acknowledges financial support from the Biotechnology and Biological Sciences Research Council.

* To whom correspondence should be addressed. Phone: (33) 169319794. Fax: (33) 169319996. E-mail: vos@enstay.ensta.fr.

‡ INSERM U451.

§ Royal Veterinary and Agricultural University and Niels Bohr Institute.

|| University of Bristol.

[1] Abbreviations: Bchl, bacteriochlorophyll; ET, electron transfer; FT, Fourier transform; RC, reaction center; SVD, singular-value decomposition; WT, wild type.

10.1021/bi000759n CCC: $19.00
Published on Web 06/24/2000

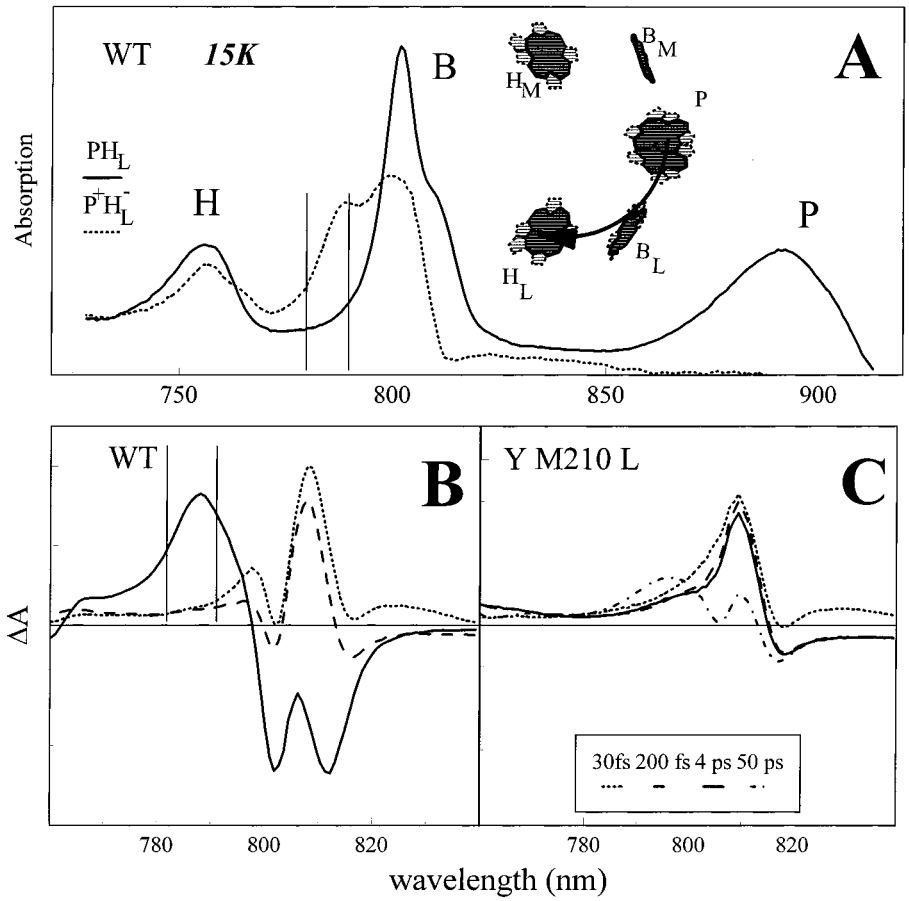

FIGURE 1: (A) The 15 K absorption spectrum of the ground state PH_L (—) and charge-separated state $P^+H_L^-$ (- - -) of WT RCs. The latter was obtained by normalizing the magic-angle transient spectrum after 8 ps to the PH_L spectrum at 880 nm, and then subtracting it from the PH_L spectrum. The inset shows the arrangement of cofactors in the bacterial RC and the direction of primary ET (arrow). For membrane-bound RCs, the view is in the plane of the membrane with the periplasmic and cytoplasmic sides of the membrane at the right- and left-hand sides of the figure, respectively. P is the primary donor bacteriochlorophyll dimer. B_L and B_M are the bacteriochlorophyll monomers, and H_L and H_M are the bacteriopheophytins, along the active (L) and inactive (M) cofactor branch, respectively. (B and C) Transient absorption spectra in the B band region for WT (B) and YM210L (C) RCs at delay times of 30 fs (- - -), 200 fs (— — —), 4 ps (—), and 50 ps (-•-•-, YM210L only). The vertical bars (A and B) denote the spectral range used to monitor the kinetics of $P^+H_2^-$ formation in this work.

signal of the B cofactors, which is a response of the ground state absorbance bands of the B cofactors to the electric field generated by the charge pair $P^+H_L^-$. In this paper, we focus on the kinetics of the B band-shift, and compare wild-type (WT) RCs with RCs that contain the mutations Phe L181 → Tyr (FL181Y) and Tyr M210 → Leu (YM210L). For both of these mutants, the frequency spectrum of vibrations set in motion by P* formation is the same as for the WT RC (*28*). However, charge separation is somewhat more rapid in the FL181Y RC than in the WT complex, but is sufficiently slow in the YM210L RC that it does not occur on the time scale of the experiments described below (*28*, *29*). Using this approach, we provide evidence for a coherent modulation of the development of the charge-separated state ($P^+H_L^-$) in WT RCs. We also present and discuss the absolute spectrum of the $P^+H_L^-$ state in the WT RC.

MATERIALS AND METHODS

Membranes were prepared from the antenna-deficient *R. sphaeroides* strain RCO1, which contains WT RCs, and from antenna-deficient strains with RCs bearing the YM210L or FL181Y mutation, as described previously (*30*, *31*). The membranes were suspended in 20 mM Tris buffer (pH 8.0) and were mixed with 50% glycerol (v/v) to an optical density of ~0.1 at the absorption maximum of the P band at ~860 nm (optical path length of 1 mm). To prereduce the quinone electron acceptor Q_A, 50 mM dithiothreitol was added. The measurements were performed at 15 K in a convection cryostat. Multicolor pump−probe spectroscopy was performed as described elsewhere (*21*). Briefly, the RCs were excited by a 30 fs (full width half-maximum) pump pulse centered at 880 nm. The transmission of the sample was monitored with a white light continuum probe pulse, compensated for group velocity dispersion and compressed to less than 15 fs over the spectral range of 770−830 nm. Spectra were recorded with a resolution of 1 nm. Scans were recorded with the pump−probe delay time varying over a 4 ps range (with 33 fs time increments) and a 50 ps range. To avoid photoselection effects, the pump and probe pulse were polarized at a magic angle (54.7°). The repetition rate was 30 Hz.

The spectral dependencies of the amplitude and phase of the Fourier transform (FT) components that modulate the kinetics were extracted from the data using a procedure employing singular-value decomposition (SVD), as described in detail elsewhere (*21*).

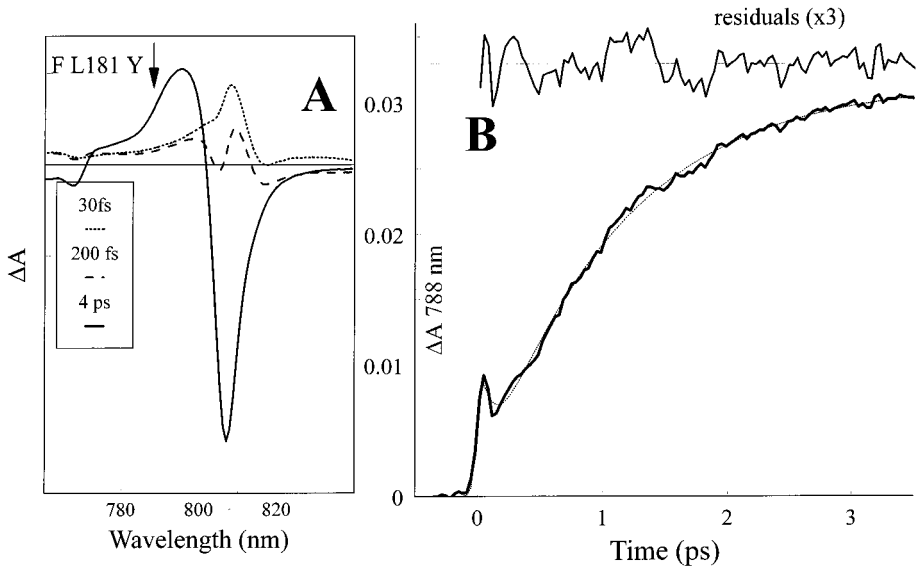

FIGURE 2: (A) Transient absorption spectra in the B band region for FL181Y RCs at delay times of 30 fs (- - -), 200 fs (— — •), and 4 ps (—). (B) Kinetics of the absorbance change at 788 nm. The thin dashed line represents a multiexponential fit [fit function being $0.008e^{(-t/30\ fs)} + 0.009e^{(-t/140\ fs)} - 0.031e^{(-t/1.0\ ps)} + 0.032$, convoluted with the instrument response function]. The upper trace shows residuals of the fit (×3).

RESULTS

The ground state absorption spectrum of the WT RC is shown in Figure 1A (solid spectrum). The absorbance band at ∼890 nm can be attributed to the pair of BChls that constitute the primary donor of electrons (P). The asymmetric band at ∼802 nm can principally be attributed to the monomeric BChls B_L and B_M, with the red shoulder carrying a small contribution from the upper exciton band of the P BChls (*32*). The band at ∼760 nm can be attributed to the H_L and H_M bacteriopheophytins.

Selected transient spectra recorded for WT and YM210L RCs are shown in panels B and C of Figure 1, respectively. At early delay times (Figure 1B, dotted spectrum), the transient spectra of the WT RC are dominated by P excited state (P*) absorption bands that appear near the ground state B absorption bands (*33*). For the YM210L mutant, the transient spectrum of P* (Figure 1C, dotted spectrum) is somewhat less structured, but the spectral evolution on the 100 fs time scale, characterized previously for the WT complex (*33*), is similar in both RCs. Between 200 fs (Figure 1B,C, dashed spectra) and 4 ps (Figure 1B,C, solid spectra), the shape of the transient spectrum hardly changes in the YM210L RC, whereas in the WT RC, a strong band-shift develops during this time interval. This shift reflects the electrochromic response of the absorption bands of the B_L and B_M BChls to charge separation. The B absorption is altered from a strong narrow band with a maximum at 802 nm and a shoulder on the red side in the neutral state (Figure 1A, solid spectrum) to a broader, net blue-shifted band with two distinct peaks at 800 and 789 nm in the $P^+H_L^-$ state (Figure 1A, dotted spectrum). The band at 789 nm is assigned to B_L because (a) in the neutral ground state this BChl absorbs somewhat more to the blue than B_M (*32*, *34*) and (b) B_L is expected to undergo the strongest electrochromic shift due to H_L^- formation. A more quantitative interpretation of the absolute spectrum of the $P^+H_L^-$ state, which has not been reported before, will be given in the Discussion.

For completeness, the 50 ps transient spectrum of the YM210L RC is also shown in Figure 1C (dotted and dashed spectrum). An electrochromic shift of the B bands is observed that is similar to that in the WT RC. This band-shift is associated with charge separation, which takes ∼190 ps in the YM210L mutant under our experimental conditions (*28*).

For the FL181Y mutant (Figure 2A), the transient spectra on the blue side of the B band are similar to those obtained with the WT RC. At the red side of the B band, the split bleaching observed in the spectra of the WT RC (Figure 1B, solid spectrum) is merged to a single bleaching centered at 807 nm (Figure 2A, solid spectrum). This merging reflects the lack of structure in the B band of the ground state spectrum of this mutant (not shown).

As reported previously in several papers, a complex pattern of oscillatory features is observed in the 790−820 nm range in experiments with WT RCs (*3*, *21*, *23*, *24*). The transient spectrum in this region includes contributions from P*-induced absorption bands, as well as shifts and possible bleachings of the B band in the P* state and in radical pair states. This congestion prohibits a reliable assignment of individual features (*21*). Oscillations with comparable amplitudes were also observed for the YM210L RC, including oscillations with frequencies down to ∼30 cm^{-1}, with a pattern somewhat different from that obtained with the WT RC. This confirms our previous interpretation that the oscillations observed in this region of the spectrum of the WT RC are, at least in part, due to P* (*21*).

In contrast, the spectral region below 790 nm is not very congested. In the P* state (Figure 1B, dotted spectrum), only a weak and broad induced absorption appears in this region. In the $P^+H_L^-$ state (Figure 1B, solid spectrum), the induced absorption that arises from the blue shift of the B band dominates the spectrum; the amplitude of this signal is an order of magnitude greater than that of the P* signal in this spectral range. The vibrational pattern in this region is also much less complex than in the 790−820 nm region. Figure 2B shows the kinetics of the change in absorbance at 788

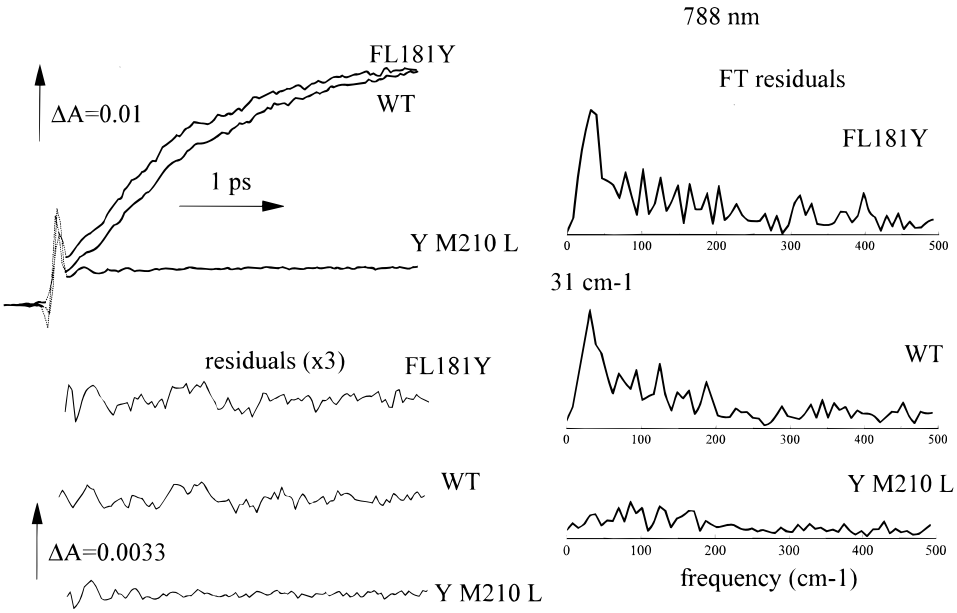

FIGURE 3: Transient kinetics at 788 nm of WT, FL181Y, and YM210L RCs and the Fourier transform of the oscillatory part of the trace obtained after subtraction of a multiexponential fit. All traces of the three types of RCs were normalized on the amplitude corresponding to full development of the band-shift. The *y*-axis scales are the same within 10%. The Δ*A* indications correspond to the WT traces.

nm for the FL181Y mutant. After an initial relaxation of ~100 fs (cf. ref *33*), the overall kinetic rise can be described with a time constant of ~1.0 ps, but it is modulated by a weak but significant oscillatory feature. Figure 3 shows that a similar modulation is observed in the corresponding kinetics of the WT RC. In both cases, the Fourier transformation of the modulation yields a peak at 30 cm^{-1} (period of ~1.0 ps), with an amplitude that amounts to at least approximately 3% of the final amplitude of the signal [the details of the modulation as extracted from the fit residuals depend somewhat on the fit parameters; however, the residuals that are shown correspond to a *minimal* amplitude of the modulation (cf. ref *6*)]. In the corresponding kinetics of the YM210L mutant RC, which reflects only P* absorption on this time scale, extremely weak modulations at higher frequencies are observed. We ascribe these weak modulations to vibrational motions on the P* potential energy surface [the frequencies found are similar to those observed in P*-stimulated emission (*28*)]. However, in this mutant, the relatively strong 30 cm^{-1} feature is clearly absent. Similar results have been obtained with other mutant RCs that have a long-lived P* state (data not shown). We note that if this 30 cm^{-1} modulation were present in the YM210L mutant, it would be easier to visualize than in the FL181Y and WT RCs. This is because in the latter case the overall rise kinetics have to be subtracted, and these have a time constant that is similar to the period of the modulation. This comparison indicates strongly that in the WT and FL181Y RCs this feature represents a modulation of the band-shift that reflects charge displacement in the transmembrane direction. In other words, a periodically oscillating component modulates the dipole sensed by the B BChls in the $P^+H_L^-$ state.

In principle, two different mechanisms can be responsible for the modulation of the B band-shift during formation of the $P^+H_L^-$ state: (a) a coherent component in the dynamics of population of the product $P^+H_L^-$ state or (b) charge oscillations in the product $P^+H_L^-$ state of the cofactor system that modulate the position of the B band with respect to its average position in the $P^+H_L^-$ state. A very schematic representation of the two situations is sketched in Figure 4. In the first case (Figure 4A), the amplitude of the band-shift signal is expected to develop in a stepwise manner, and the amplitude dependence of the oscillation is expected to be the same as that of the band-shift, with opposing phase at either side of the zero crossing point of the band-shift signal. In the second case (Figure 4B), the disappearance and phase shift of the oscillation are expected to occur at the maximum of the position of the B band in the $P^+H_L^-$ state.

The spectral characteristics of the 30 cm^{-1} FT peak in the B band region (Figure 5A) are clearly consistent with the first mechanism and not with the second. When $\lambda < 790$ nm, the 30 cm^{-1} oscillatory modulation obtained for the WT and FL181Y RCs is much stronger than any other oscillatory modulation, whereas in the YM210L RC, all features are very small. In the 770−790 nm region, the wavelength dependence of the amplitude of the 30 cm^{-1} peak is similar to the spectrum of the band-shift signal. Furthermore, the corresponding phase in this region is approximately constant (Figure 5B). When $\lambda > 790$ nm, the spectral dependence of the oscillation is complex (*21*) due to contributions from P*. When $\lambda > 815$ nm, the amplitude dependence of the 30 cm^{-1} feature tracks the shape of the band-shift and is opposite in phase with respect to the region when $\lambda < 790$ nm (not shown). This is consistent with our interpretation in terms of a coherent component in the dynamics of population of the $P^+H_L^-$ state (cf. Figure 4). However, we also find that ~30 cm^{-1} features contribute significantly to the kinetics of the YM210L mutant in the spectral range above 790 nm (including near 805 nm; see the Discussion), and that this region displays complicated multipeak amplitude characteristics. These findings indicate that modulation of P* absorption also contributes when $\lambda > 790$ nm. As a result, the region between 770 and 790 nm is the only spectral region where the band-shift kinetics can be reliably analyzed without significant interference from other components.

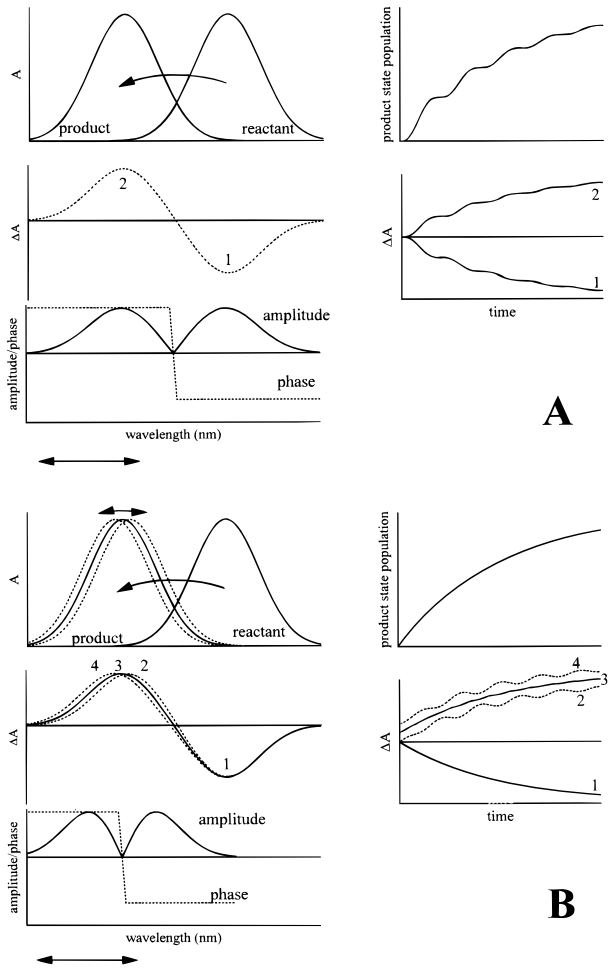

FIGURE 4: Schematic predictions of the wavelength dependence of oscillatory features in the B band region originating from (A) an oscillatory modulation of the "rate" of charge separation and (B) charge oscillations in the product state. (A) The formation of the product state generates an electric field that leads to a band-shift (upper and middle left). The kinetics of product state formation are modulated by oscillations (upper right), and this leads to oscillations in both the bleaching and the induced absorption part of the band-shift, with opposite phases in the Δ*A* signal (lower right). The corresponding phase and amplitude dependence of the fundamental frequency oscillatory component follows the band-shift (lower left). (B) The formation of the product state generates an electric field, superimposed on which is an oscillatory electric field generated by charge oscillations in the product state. This leads to a modulation of the position of the shifted band (upper left). The corresponding band-shift signal is therefore modulated, and for relatively small charge oscillations, this modulation predominantly affects the induced absorption part of the band-shift (middle left). The dynamics of product state formation are smooth (upper left). The bleaching part of the Δ*A* signal is also smooth (lower right), but the induced absorption part is modulated at either side of the average position of the band-shift (lower right, curves 3 and 4 are vertically displaced for clarity). The corresponding phase and amplitude dependence of the fundamental frequency oscillatory component displays a similar shape as in panel A, but is centered around the maximum of the band-shift signal rather than its zero-crossing point (lower left). The double-sided arrows below both schemes indicate approximately the spectral region where the 30 cm^{-1} component can be analyzed in our experiments.

DISCUSSION

We have studied in detail the spectral characteristics of oscillatory features in the electrochromic band-shift of the BChl monomers that probe charge displacements within the bacterial RC. A 30 cm^{-1} modulation was detected in the kinetics of the WT and FL181Y RCs, but not in the kinetics of the YM210L mutant RC, showing that it is not due to coherent vibrational motion on the P* potential energy surface. The spectral characteristics further associate the feature with the population of the $P^+H_L^-$ state, and we conclude that it reflects a modulation of the development of the electric field associated with the $P^+H_L^-$ product state(s) of the primary ET reaction. Our findings provide the first unambiguous evidence for a coherent component in a biological charge displacement reaction.

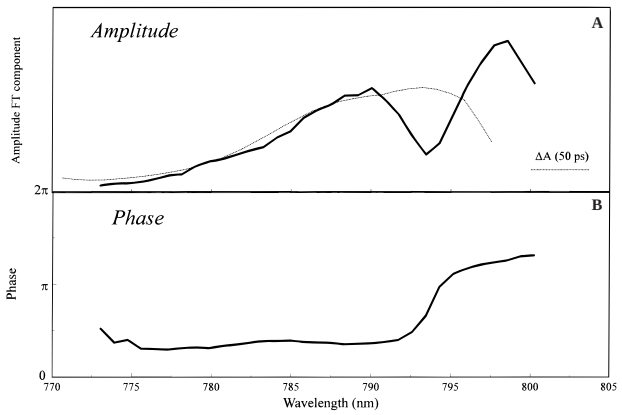

FIGURE 5: Amplitude (A) and phase (B) of the 30 cm^{-1} FT feature as a function of wavelength in the B band spectral region of WT RCs (solid lines). The dashed line in panel A represents the transient absorption spectrum at 50 ps.

We stress that use of the electrochromic effect on the absorption of the B cofactors, which are not directly involved in the $P^+H_L^-$ charge pair, has the advantage of monitoring only the effect of the reaction (the electric field induced by the charge pair), and therefore, modulations in this effect can be directly ascribed to modulation of the charge displacement. In contrast, the relatively weak absorption bands of the product states can be modulated by population dynamics as well as motions within such states, which complicates the interpretation (cf. ref *21*).

Insights from the $P^+H_L^-$ Spectrum. The position of the B band is sensitive to the local electric field that is determined by the distribution of charge in the RC. Steffen et al. (*34*) have used this to estimate the effective dielectric constant, ϵ_{eff}, in different regions of the protein from the spectrum of the $P^+Q_A^-$ state, using the relation

$$\Delta\nu = -\Delta\mu\cdot\mathbf{F} \qquad (1)$$

where $\Delta\nu$ is the electrochromic shift and $\Delta\mu$ the difference in permanent dipole moment for the optical transition. The term **F** is the electric field, which is given by

$$\mathbf{F} = \epsilon\sum_i \frac{q_i}{r_i^2}\hat{\mathbf{r}}_i \qquad (2)$$

where q_i is a charge located a distance r_i from the chromophore and $\hat{\mathbf{r}}_i$ is the unit vector that connects q_i and the probe charge on the chromophore. The results of calculations based on the electrochromic shifts of B_L and B_M, using the methodology outlined in ref *34*, are given in Table 1. For the effect of the $P^+H_L^-$ charge pair on the B_L absorption,

Table 1: Calculated Electrochromic Shifts of B_L and B_M for the Radical Pair State $P^+H_L^-$ and Comparison with the Measured Shift of B_L[a]

	$P^+H_L^-$ [b,c]			$P_L^+P_M^-$ [c]
	$\Delta\nu_{calc}(\epsilon=1)$ (cm^{-1})[d]	$\Delta\nu_{obs}$ (cm^{-1})	ϵ_{eff}	$\Delta\nu_{calc}(\epsilon=1)$ (cm^{-1})[d]
B_L	507−660	220	2.3−3.0	−102 to 51
B_M	130−280	*e*		−124 to 150

[a] The calculations were performed according to ref *34*, using the values therein for $|\Delta\mu|$ and the angles ζ_a between $\Delta\mu$ and the vector connecting the nitrogen atoms of rings I and III of bacteriochlorophyll. The coordinates for the RC were taken from the X-ray structure of Ermler et al. (*52*) (file 1PCR, Protein Data Bank). [b] The charge distribution within P^+ was taken to be $^2/_3$ on P_L and $^1/_3$ on P_M (*37*). [c] Within the chromophores, the charges were evenly distributed among the four nitrogen atoms. [d] The range of values corresponds to varying the angles between $\Delta\mu$ and the vector connecting the nitrogen atoms of rings I and III over $\pm\zeta_a$ within the plane of the macrocycle. [e] The position of the Q_Y B_M absorption in the neutral ground state is uncertain due to its overlap with the upper exciton transition of P (*32*); therefore, we have not estimated the experimental electrochromic shift.

we calculate a value for $\Delta\nu$ assuming a dielectric constant ϵ of 1 [$\Delta\nu(\epsilon=1)$] in the range of 507−660 cm^{-1}. As discussed above, comparison of the PH_L and $P^+H_L^-$ spectra shows that the B_L absorption maximum shifts from 802 to 788 nm ($\Delta\nu$ = 220 cm^{-1}); therefore, we estimate that the average effective dielectric constant (ϵ_{eff}) for this transition is in the range of 2.3−3.0. This is somewhat lower than the range of values estimated by Steffen et al. (*34*) for the $P^+Q_A^-$ charge pair, suggesting that the protein between H_L and Q_A has a relatively high effective dielectric constant. The presence of several water molecules in the vicinity of Q_A (*35*) may be related to this observation.

Similar calculations can be performed for other charge pairs. In particular, we estimate a value for $\Delta\nu(\epsilon=1)$ in the range of −102 to 51 cm^{-1} for the effect of a putative charge pair $P_L^+P_M^-$ on the absorption of B_L (Table 1). Thus, if it is assumed that the value of ϵ_{eff} for the field at B_L is the same in the presence of $P_L^+P_M^-$ as in the presence of $P^+H_L^-$, the full $P_L^+P_M^-$ charge displacement is expected to give a signal of, at the very most, 20% of the B_L band-shift that is caused by the $P^+H_L^-$ charge displacement.

The coherent vibrational modes set in motion by population of the P* state will probably include relative motions of chromophores, and it is expected that the latter are predominantly "dimer-type", i.e., relative motions of P_L and P_M (*36*). If such motions are transferred to the product state $P^+H_L^-$, the associated charge oscillation would be expected to correspond to only a small fraction of that of the $P_L^+P_M^-$ dipole; the charge asymmetry on P amounts to only $\sim^1/_3$ of an elementary charge, at least in the steady state (*37*), and the amplitude of the motions can only amount to a fraction of the P_L-P_M distance. Altogether, unrealistically high values for the amplitude of the motions (tens of percents of the P_L-P_M equilibrium distance) would have to be assumed to make them detectable in our experiments. This reasoning provides further support for our conclusion that the observed oscillations of the B band-shift do not originate from modulation of the position of the B band in the $P^+H_L^-$ state.

Origin of the Modulation of the B Band-Shift. As discussed above, the observed ∼1 ps period modulation of the development of the transmembrane potential sensed by the BChl monomers reflects a modulation in the speed of ET from P to H_L. This modulation is presumably due to periodic structural rearrangements of the protein−cofactor system, which modulate the population of the transition zone between the precursor state and the $P^+H_L^-$ state. There has been extensive debate (*17*, *38*−*40*) about whether this precursor state is P*, according to a one-step model for ET, or $P^+B_L^-$ (formed from P*), according to a two-step model. The only documented periodic variations which could be responsible for modulation of formation of the $P^+H_L^-$ charge pair are the vibrational motions that are activated by P* formation (*41*). In the following, we will discuss the possible involvement of vibrational motions associated with the P* state in the modulation of the population of the product state(s) of ET.

First, we discuss the presence of a coherent vibrational mode with a fundamental frequency at ∼30 cm^{-1} in the P* state. Previous stimulated (*21*, *28*, *36*, *41*) and spontaneous (*42*) emission studies have demonstrated that a manifold of low-frequency vibrational modes is set in motion upon formation of the P* state, generally consistent with coupling of such modes to the P → P* transition observed with resonance Raman (*43*, *44*) and hole-burning spectroscopy (*45*, *46*). Whereas the main modes are in the 70−160 cm^{-1} region, very low-frequency modes are also present. As has been discussed elsewhere (*41*, *42*), the precise characteristics of these modes are difficult to assess, because their periods are similar to the overall rate of decay of the P* state in the WT RC (and in the FL181Y mutant). In our analysis of WT RCs, a peak at ∼15 cm^{-1} was found in the FT spectrum of fundamental frequencies but an oscillator strength at ∼30 cm^{-1} was also present (*41*) and a Raman mode of 34 cm^{-1} has been reported (*43*). For the YM210L mutant, where P* does not decay on the time scale of a few picoseconds, assessment of the low-frequency part of the vibrational spectrum is more reliable because the longer-lasting oscillations lead to improved spectral resolution. Close inspection of the FT spectrum of the fundamental frequencies in the YM210L RC (Figure 3 in ref *28*) reveals a distinct feature at ∼30 cm^{-1}, but the relative amplitude of this feature is very small. Thus, whereas vibrational motions with a fundamental frequency of ∼30 cm^{-1} are set in motion upon impulsive formation of P*, the amplitude of their coupling to the P → P* transition is very small.

Another possibility is that the 30 cm^{-1} modulation of the charge separation originates from a beat between higher-frequency modes. The strongest distinct bands in the FT spectrum of P* are located at 92, 122, and 153 cm^{-1} (*41*), i.e., at 30 cm^{-1} intervals, indicating that this is indeed a more likely possibility.

At this point, we wish to note that, a priori, lower-frequency periodic modulations of the rate of ET will lead to larger amplitude modulations of the product state population than higher-frequency periodic modulations. The reasons for this are outlined in the Appendix. Therefore, it is possible that higher-frequency components do modulate the population of the product state (this is likely to be the case if the 30 cm^{-1} feature corresponds to a beat between higher-frequency modes), but these modulations are too weak to be detected in the experiments presented here.

In a two-step model ($P^* \rightarrow P^+B_L^- \rightarrow P^+H_L^-$), the overall similarity of the kinetics for P* decay and $P^+H_L^-$ appearance

implies that $P^+B_L^-$ decay must be much more rapid than its population. In our 15 K experiments, where P* decays in ~1 ps, the dwell time of the $P^+B_L^-$ state would therefore correspond to only a small fraction of the period (1 ps) of a 30 cm^{-1} mode.[2] It is therefore difficult to envisage how coherent motion on the $P^+B_L^-$ potential energy surface with a frequency of 30 cm^{-1} could be at the origin of the observed modulation of $P^+H_L^-$ formation. However, in an alternative mechanism where population of $P^+B_L^-$ from P* leads to rapid movement of the system to the transfer zone with the $P^+H_L^-$ state, and to subsequent near-adiabatic crossing, a modulation of $P^+B_L^-$ formation could be transferred to a modulation of $P^+H_L^-$ formation without much dephasing. Such a mechanism has been described by Almeida and Marcus (*14*) for the more general case of a donor−bridge−acceptor system. For the WT RC, the recent ab initio calculation of strong electronic coupling (122 cm^{-1}) between $P^+B_L^-$ and $P^+H_L^-$ (*49*) would also be in agreement with such a mechanism.

Comparison with Other Work. The possible coupling of coherent motion to primary ET has been experimentally investigated in a number of studies. Streltsov and co-workers (*22*, *23*) have suggested that very low-frequency (8−31 cm^{-1}) FT components observed in the B band region (near 805 nm) reflect coherent B_L^- formation. As discussed elsewhere (*21*), and in this report, other mechanisms are also likely to give rise to such components in this congested spectral region. Our observation of such low-frequency components in the spectral region near 805 nm in YM210L mutant RCs, where due to slow ET only the P* state is populated on the time scale of a few picoseconds, further points to strong contributions from P* in the observations reported in refs *22* and *23*, which complicates the interpretation of these results.

Spörlein and co-workers have analyzed oscillations observed in the 1020 nm band assigned to B_L^- at room temperature (*26*). This work indicated that the dominant 135 cm^{-1} feature arose from stimulated emission rather than B_L^- modulation, and was inconclusive about lower-frequency features.[3] Our work is consistent with this, as we also do not observe modulation of the ET kinetics in the 90−160 cm^{-1} frequency region.

Mechanism of Primary Electron Transfer. It is useful to place our results in the framework of adiabatic versus nonadiabatic primary ET. Analysis of the temperature dependence of the overall rate of ET in bacterial RCs in terms of a thermally populated, single-mode, nonadiabatic, activationless model yielded a mode frequency in the range of 25−80 cm^{-1} (*20*). This range is on the same order of magnitude as the 30 cm^{-1} mode that we propose to be involved in ET. Yet a number of observations indicate that this model does not fully cover all of the features of primary ET at low temperatures.

(1) At a reaction "frequency" of 1 ps^{-1} and an overall reaction "rate" of ~1 ps, the surface crossing probability per passage in the crossing zone should be ~70% and, in contrast to the situation at room temperature, the nonadiabatic condition (low probability of crossing) is therefore not well fulfilled. It is conceivable that the reaction changes from an essentially nonadiabatic regime at room temperature to a near-adiabatic regime at cryogenic temperatures (cf. ref *50*).

(2) The mode(s) which gives rise to the coherent component in primary ET is presumably populated by the P → P* transition. Vibrational relaxation takes place on a time scale that is longer than ET (*28*), and hence, these vibrational motions are not in thermal equilibrium with the "bath" modes. This implies that at cryogenic temperatures, where thermal motions are frozen out, significant motion along coordinates coupled to the ET reaction persists. Hence, to explain the extreme rapidness of this process at low temperatures, it is not necessary to invoke ET occurring from the equilibrium position of the P* potential energy surface (corresponding to a completely "activationless" reaction in a picture of ET driven by thermal motions).

(3) The amplitude of the observed modulation of primary ET is small. Within the framework of a single-mode model, this would imply (a) that the modulation of the rate of ET as a function of nuclear coordinates is weak, corresponding to a "transition zone" with a width comparable to the amplitude of the motions, or (b) that a frequency-dispersed (around 30 cm^{-1}) distribution of vibrational modes couples to ET. However, as discussed above, multimode coupling [as suggested previously in theoretical work (*51*)] with the 30 cm^{-1} component representing the ensemble effect (difference frequency beat) of more than one mode appears to be a more likely possibility. Using more extensive modeling, we are presently exploring these various possibilities.

APPENDIX

Ando and Sumi (*15*) have recently treated ET in RCs according to a semiclassical Landau−Zener picture, with explicit inclusion of coherent motions in the excited state. Oscillatory features in the ET rate $k_{ET}(t)$ appear through a complicated dependence on the "displacement along the reaction coordinate" sum $Q(t)$:

$$Q(t) = \sum_j \hbar\omega_j \Delta_j \Delta'_j \cos(\omega_j t) \qquad \text{(A1)}$$

and its time derivative

$$\dot{Q}(t) = -\sum_j \hbar\omega_j \Delta_j \Delta'_j \sin(\omega_j t) \qquad \text{(A2)}$$

where Δ_j is the dimensionless displacement of the jth mode with frequency ω_j between the ground and excited state and Δ'_j is the displacement between the excited and product states. As expected, only vibrations that are at the same time excited by the P → P* transition ($\Delta_j \neq 0$) and coupled to ET ($\Delta'_j \neq 0$) contribute.

A calculation of the oscillations in the P* → P stimulated emission along similar lines (C. Rischel, M. H. Vos, and

[2] Analysis of the overall evolution of our present full spectral data using 30 fs pulses did not identify any exponential phases characteristic of $P^+B_L^-$. This is consistent with several previous reports of low-temperature experiments using a longer pump pulse (*33*, *47*); however, Lauterwasser et al. (*48*) reported $P^+B_L^-$ decay in 300 ± 150 fs at 25 K with a 300 fs time resolution.

[3] In a very recent paper by Yakovlev and co-workers (*27*), measurements similar to those in ref *26* reported only for 1020 nm were interpreted as population of a transition zone between P* and $P^+B_L^-$ without actual surface crossing (termed "reversible charge separation"). The spectroscopic characterization of ref *26*, indicating that the oscillations at 1020 nm arise from the P*-stimulated emission signal rather than from absorption of a charge-separated state, seems inconsistent with such a mechanism.

J.-L. Martin, unpublished results) reveals that the relevant sum over modes in this case is

$$\sum_j \hbar\omega_j \Delta_j^2 \cos(\omega_j t) \tag{A3}$$

Comparison of these analyses shows that the dependence on ω_j has the same form, so a priori, we expect low-frequency vibrations to play similar roles in the modulation of the rate of ET and in the modulation of stimulated emission.

The oscillations that we measure in this work are those of the population term. We can in general write the ET rate as a sum of oscillating terms (including frequency sum/difference terms of all orders):

$$k_{ET}(t) = k_0\{1 + \sum_n [A_n \cos(\Omega_n t) + B_n \sin(\Omega_n t)]\} \tag{A4}$$

The probability $p(t)$ of finding the molecule in the product state is then

$$p(t) = 1 - \exp\left(-k_0\left\{t + \sum_n \frac{1}{\Omega_n}[A_n \sin(\Omega_n t) - B_n \cos(\Omega_n t)]\right\}\right) \tag{A5}$$

The key feature of this expression is the dependence on the reciprocal of the frequency. This implies that the low-frequency terms are strongly favored.

ACKNOWLEDGMENT

We thank Marie-Louise Groot and Jacques Breton for reading the manuscript.

REFERENCES

1. Vos, M. H., and Martin, J.-L. (1999) *Biochim. Biophys. Acta 1411*, 1−20.
2. Dexheimer, S. L., Wang, Q., Peteanu, L. A., Pollard, W. T., Mathies, R. A., and Shank, C. V. (1992) *Chem. Phys. Lett. 188*, 61−66.
3. Vos, M. H., Lambry, J.-C., Robles, S. J., Youvan, D. G., Breton, J., and Martin, J.-L. (1991) *Proc. Natl. Acad. Sci. U.S.A. 88*, 8885−8889.
4. Wang, Q., Schoenlein, R. W., Peteanu, L. A., Mathies, R. A., and Shank, C. V. (1994) *Science 266*, 422−424.
5. Zhu, L., Sage, J. T., and Champion, P. M. (1994) *Science 266*, 629−632.
6. Liebl, U., Lipowski, G., Négrerie, M., Lambry, J.-C., Martin, J.-L., and Vos, M. H. (1999) *Nature 401*, 181−184.
7. Skourtis, S. S., da Silva, A. J. R., Bialek, W., and Onuchic, J. N. (1992) *J. Phys. Chem. 96*, 8034−8041.
8. Jean, J. (1994) *J. Chem. Phys. 101*, 10464−10473.
9. Jean, J., and Fleming, G. R. (1995) *J. Chem. Phys. 103*, 2092−2101.
10. Franzen, S., and Martin, J.-L. (1995) *Annu. Rev. Phys. Chem. 46*, 453−487.
11. Alden, R. G., Cheng, W. D., and Lin, S. H. (1992) *Chem. Phys. Lett. 194*, 318−326.
12. Wolfseder, B., Seidner, L., Stock, G., and Domcke, W. (1997) *Chem. Phys. 217*, 275−287.
13. Gehlen, J. N., Marchi, M., and Chandler, D. (1994) *Science 263*, 499−502.
14. Almeida, R., and Marcus, R. A. (1990) *J. Phys. Chem. 94*, 2978−2985.
15. Ando, K., and Sumi, H. (1998) *J. Phys. Chem. B 102*, 10991−11000.
16. Ashkenazi, G., Kosloff, R., and Ratner, M. A. (1999) *J. Am. Chem. Soc. 121*, 3386−3395.
17. Hoff, A. J., and Deisenhofer, J. (1997) *Phys. Rep. 287*, 1−247.
18. Martin, J.-L., Breton, J., Hoff, A. J., Migus, A., and Antonetti, A. (1986) *Proc. Natl. Acad. Sci. U.S.A. 83*, 957−961.
19. Woodbury, N. W., Becker, M., Middendorf, D., and Parson, W. W. (1985) *Biochemistry 24*, 7516−7521.
20. Fleming, G. R., Martin, J.-L., and Breton, J. (1988) *Nature 333*, 190−192.
21. Vos, M. H., Jones, M. R., and Martin, J.-L. (1998) *Chem. Phys. 233*, 179−190.
22. Streltsov, A. M., Yakovlev, A. G., Shkuropatov, A. Y., and Shuvalov, V. A. (1996) *FEBS Lett. 383*, 129−132.
23. Streltsov, A. M., Aartsma, T. J., Hoff, A. J., and Shuvalov, V. A. (1997) *Chem. Phys. Lett. 266*, 347−352.
24. Streltsov, A. M., Vulto, S. I. E., Shkuropatov, A. Ya., Hoff, A. J., Aartsma, T. J., and Shuvalov, V. A. (1998) *J. Phys. Chem. B 102*, 7293−7298.
25. Groot, M.-L., Yu, J.-Y., Agarwal, R., Norris, J. R., and Fleming, G. R. (1998) *J. Phys. Chem. B 102*, 5923−5931.
26. Spörlein, S., Zinth, W., and Wachtveitl, J. (1998) *J. Phys. Chem. B 102*, 7492−7496.
27. Yakovlev, A. G., Shkuropatov, A. Y., and Shuvalov, V. A. (2000) *FEBS Lett. 466*, 209−212.
28. Vos, M. H., Jones, M. R., Breton, J., Lambry, J.-C., and Martin, J.-L. (1996) *Biochemistry 35*, 2687−2692.
29. Chan, C.-K., Chen, L. X.-Q., DiMagno, T. J., Hanson, D. K., Nance, S. L., Schiffer, M., Norris, J. R., and Fleming, G. R. (1991) *Chem. Phys. Lett. 176*, 366−372.
30. Jones, M. R., Visschers, R. W., van Grondelle, R., and Hunter, C. N. (1992) *Biochemistry 31*, 4458−4465.
31. Jones, M. R., Heer-Dawson, M., Mattioli, T. A., Hunter, C. N., and Robert, B. (1994) *FEBS Lett. 339*, 18−24.
32. Vos, M. H., Rischel, C. R., Breton, J., Martin, J.-L., Ridge, J. P., and Jones, M. R. (1998) *Photosynth. Res. 55*, 181−187.
33. Vos, M. H., Lambry, J.-C., Robles, S. J., Youvan, D. G., Breton, J., and Martin, J.-L. (1992) *Proc. Natl. Acad. Sci. U.S.A. 89*, 613−617.
34. Steffen, M. A., Lao, K., and Boxer, S. G. (1994) *Science 264*, 810−816.
35. Fritsch, G., Kampmann, L., Kapaun, G., and Michel, H. (1998) *Photosynth. Res. 55*, 127−132.
36. Rischel, C., Spiedel, D., Ridge, J. P., Jones, M. R., Breton, J., Lambry, J.-C., Martin, J.-L., and Vos, M. H. (1998) *Proc. Natl. Acad. Sci. U.S.A. 95*, 12306−12311.
37. Lendzian, F., Huber, M., Isaacson, R. A., Endeward, B., Bönigk, B., Möbius, K., Lubitz, W., and Feher, G. (1993) *Biochim. Biophys. Acta 1183*, 139−160.
38. Zinth, W., and Kaiser, W. (1993) in *The Photosynthetic Reaction Center* (Deisenhofer, J., and Norris, J. R., Eds.) Vol. II, pp 71−88, Academic Press, San Diego.
39. Kirmaier, C., and Holten, D. (1993) in *The Photosynthetic Reaction Center* (Deisenhofer, J., and Norris, J. R., Eds.) Vol. II, pp 49−70, Academic Press, San Diego.
40. Woodbury, N. W., and Allen, J. P. (1995) in *Anoxygenic Photosynthetic Bacteria* (Blankenship, R. E., Madigan, M. T., and Bauer, C. E., Eds.) Kluwer, Dordrecht, The Netherlands.
41. Vos, M. H., Jones, M. R., Hunter, C. N., Breton, J., Lambry, J.-C., and Martin, J.-L. (1994) *Biochemistry 33*, 6750−6757.
42. Stanley, R. J., and Boxer, S. G. (1995) *J. Phys. Chem. 99*, 859−863.
43. Cherepy, N. J., Shreve, A. P., Moore, L. J., Franzen, S., Boxer, S. G., and Mathies, R. A. (1994) *J. Phys. Chem. 98*, 6023−6029.
44. Czarnecki, K., Diers, J. R., Chynwat, V., Erickson, J. P., Frank, H. A., and Bocian, D. F. (1997) *J. Am. Chem. Soc. 119*, 415−426.
45. Lyle, P. A., Kolaczkowski, S. V., and Small, G. R. (1993) *J. Phys. Chem. 97*, 6924−6933.
46. Middendorf, T. R., Mazzola, L. T., Gaul, D. F., Schenck, C. C., and Boxer, S. G. (1991) *J. Phys. Chem. 95*, 10142−10151.

47. Woodbury, N. W., Peloquin, J. M., Alden, R. G., Lin, X., Lin, S., Taguchi, A. K. W., Williams, J. C., and Allen, J. P. (1994) *Biochemistry 33*, 8101−8112.
48. Lauterwasser, C., Finkele, U., Scheer, H., and Zinth, W. (1991) *Chem. Phys. Lett. 183*, 471−477.
49. Zhang, L. Y., and Friesner, R. A. (1998) *Proc. Natl. Acad. Sci. U.S.A. 95*, 13603−13605.
50. Zinth, W., Huppmann, P., Arlt, T., and Wachtveitl, J. (1998) *Philos. Trans. R. Soc. London A356*, 465−476.
51. Warshel, A., Chu, Z. T., and Parson, W. W. (1989) *Science 266*, 112−116.
52. Ermler, U., Fritzsch, G., Buchanan, S. K., and Michel, H. (1994) *Structure 2*, 925−936.

BI000759N